Research Article

Differentiation of MSC and annulus fibrosus cells on genetically-engineered silk fleece-membrane-composites enriched for GDF-6 or TGF-β3†

Daniela A Frauchiger[1], Silvan R Heeb[1,2,3], Rahel D May[1], Michael Wöltje[4], Lorin M Benneker[5], Benjamin Gantenbein[1]

[1]Institute for Surgical Technology and Biomechanics, University of Bern, CH-3014 Bern, Switzerland

[2]Department of Hematology and Central Hematology Laboratory, Inselspital, Bern University Hospital, University of Bern, CH-3010 Bern, Switzerland

[3]Department for BioMedical Research, University of Bern, CH-3010 Bern, Switzerland

[4]Institute of Textile Machinery and High Performance Material Technology, TU Dresden, DE-01069 Dresden, Germany

[5]Department of Orthopaedic Surgery and Traumatology, Inselspital, Bern University Hospital, University of Bern, CH-3010 Bern, Switzerland

†This article has been accepted for publication and undergone full peer review but has not been through the copyediting, typesetting, pagination and proofreading process, which may lead to differences between this version and the Version of Record. Please cite this article as doi: [10.1002/jor.23778]

Additional Supporting Information may be found in the online version of this article.

Received 3 July 2017; Revised 15 September 2017; Accepted 13 October 2017

Journal of Orthopaedic Research

DOI 10.1002/jor.23778

Corresponding Author:
Prof. Dr. Benjamin Gantenbein
Tissue and Organ Mechanobiology
Institute for Surgical Technology and Biomechanics,
Stauffacherstrasse 78
3014 Bern
Switzerland
E-mail: Benjamin.Gantenbein@istb.unibe.ch
Phone: +41 31 631 59 51
Running title: GDF6-enriched Silk for IVD Repair

AUTHORS CONTRIBUTIONS STATEMENT

F. DA., H. S. and M. RD. performed the laboratory work. W. M. was responsible for design and generation of transgenic silkworms, provided input on the silk and edited and approved the manuscript. B. LM. provided clinical donor material presented in this article and edited and approved the manuscript. G. B. provided funding, designed the research plan and supervised the research work. All authors approved the final version of the manuscript.

ABSTRACT

Intervertebral disc (IVD) repair is a high-priority topic in our active and increasingly ageing society. Since a high number of people are affected by low back pain treatment options that are able to restore the biological function of the IVD are highly warranted. Here, we investigated whether the feasibility of genetically-engineered (GE)-silk from *Bombyx mori* containing specific growth factors to precondition human bone-marrow derived mesenchymal stem cells (hMSC) or to activate differentiated human annulus fibrosus cells (hAFC) prior transplantation or for direct repair on the IVD.
Here, we tested the hypothesis that GE-silk fleece can thrive human hMSC towards an IVD-like phenotype. We aimed to demonstrate a possible translational application of good manufacturing practice (GMP)-compliant GE-silk scaffolds in IVD repair and regeneration. GE-silk with growth and differentiation factor 6 (GDF-6-silk) or transforming growth factor β3 (TGF-β3, TGF-β3-silk) and untreated silk (cSilk) were investigated by DNA content, cell activity assay and glycosaminoglycan (GAG) content and their differentiation potential by qPCR analysis.
We found that all silk types demonstrated a very high biocompatibility for both cell types, i.e., hMSC and hAFC, as revealed by cell activity, and DNA proliferation assay. Further, analyzing qPCR of marker genes revealed a trend to differentiation towards an NP-like phenotype looking at the *Aggrecan*/*Collagen 2* ratio which was around 10:1. Our results support the conclusion that our GE-silk scaffold treatment approach can thrive hMSC towards a more IVD-like phenotype or can maintain the phenotype of native hAFC. This article is protected by copyright. All rights reserved

Keywords: Silk; growth and differentiation factor 6; bone morphogenic protein 13;

transforming growth factor β3; intervertebral disc

INTRODUCTION

Current treatments for the restoration of the intervertebral disc (IVD) are, in a classical sense, to remove the disc following the unscientific phrase “no disc – no pain”. Biological repair methods would be desirable over pure mechanical methods, which are known to cause a high rate of post-operative complications such as IVD degeneration of adjacent segments.[1]

The lack of biological repair approaches can be accounted for by the IVDs unique composition that allows for six degree of freedom motion consisting of fibrous outer annulus fibrosus (AF) and gelatinous nucleus pulposus (NP) tissue in the core. Additionally, repair is aggravated by nutrient and oxygen supply that mainly occurs through the cartilaginous endplate (EP) and thus creates a harsh environment for cells of repetitive loading and torsion, low oxygen content and limited nutrients.[2,3] It is generally accepted that the IVD possesses only a very limited self-healing potential and thus regeneration approaches might be very challenging.[4,5]

Over the last years silk gained in importance in the orthopedic research due to its versatility and high abundance[6] and its high cyto-compatibility.[7] Along with its own properties e.g. high tensile strength, biocompatibility and advancing technology to further tailor the silk, it advanced towards the field of tissue engineering. For example, silk is currently used for repair and regeneration of distinct tissues e.g. in anterior cruciate ligament regeneration, where it is used alone or in combination with other materials.[8] Moreover, silk is used in bone,[9-12] where also other silk types than of *Bombyx mori* (Linnaeus, 1758, Lepidoptera: Bombycidae) were used. Also in IVD repair and regeneration silk is an emerging player,[13] specifically for NP restoration[14,15]

or AF repair.[16-19] Silk is a natural material mainly obtained from insects and spiders, with the "silk worm" *B. mori* as one of the biggest producers. *B. mori* larvae have been cultured for over thousand years in sericulture and used for fabrics.[20] As silk alone is suspected not to be able to induce repair or regeneration it is often used as carrier for drugs or combined with other materials that serve as drug carrier.[21]

In order to induce transformation or maintenance of IVD phenotype; members of the transforming growth factor (TGF) superfamily play a pivotal role.[22] It was shown that growth and differentiation factor 6 (GDF-6), also known as bone morphogenic protein 13, tends to induce discogenic differentiation[23] or limit the damage caused by IVD degeneration and is a possible candidate for IVD therapy.[24] GDF-5 is often mentioned along with GDF-6 because they are both members of the same family and they both seem to show beneficial effects on IVD repair/regeneration and induction of discogenic differentiation when either used alone or in combination.[25-27] Recently, it was also shown that a possible synergy between TGF-β1 and GDF-5 exists that drives differentiation of mesenchymal stem cells towards NP-like cells.[22]

The aim of this study was to assess the differentiation potential of novel-type of genetically-engineered fleece-membrane silk composites containing a human recombinant (rh) growth factor, such as GDF-6 or TGF-β3 on human primary bone-marrow derived mesenchymal stem cells (hMSCs) towards the IVD-like phenotype was assessed. Furthermore, the potential of these materials to maintain the phenotype of human annulus fibrosus cells was investigated as these cells are in direct contact in the IVD. *In vivo* cell cytocompatibility and differentiation was assessed in 3D culture on GE-silk fleece-membrane composites.

METHODS

Human mesenchymal stem cell isolation

Primary human mesenchymal stem cells (hMSC) were isolated from bone marrow aspirates from vertebrae of five patients undergoing spinal surgery with written ethical consent. hMSC were isolated by density centrifugation using Histopaque 1077 (Sigma-Aldrich, Buchs, Switzerland) and expanded up to passage one in α-Minimum Essential Medium (α-MEM) supplemented with 10 % fetal calf serum (FCS) and 2.5 ng/mL basic fibroblast growth factor.[28]

Human annulus fibrosus cell isolation

Primary cells were isolated from five patients undergoing spinal surgery with their written consent. Tissue was subjected to a mild two-step digestion protocol consisting of 1 h incubation with pronase (1.88 mg/mL, Roche Life Science, Rotkreuz, Switzerland) followed by overnight digestion with collagenase type 2 (128 U/mL, Worthington Biochemical Corporation, London, UK). The next day, the cells were filtered through a 100 μm strainer (Falcon, Becton & Dickinson, Inc., Brussels, Belgium). The hAFC were subsequently expanded up to passage one to two, respectively, in Low Glucose Dulbecco's Modified Eagle's Medium (LG-DMEM) supplemented with 10 % FCS.

Silk scaffolds

Silk scaffolds were produced by Spintec Engineering GmbH, Aachen, Germany. In short, *B. mori* larvae were cultured in sterile sericulture and infected with baculovirus causing incorporation of desired growth factor into silk fibroin,[29] see Fig. 1 modified with permission according to Kato et al. (2010).[30] Silk was directly harvested from silk

glands to reduce contamination with sericin to a minimum. This was important in the production, as sericin is known to cause allergic reaction in the human body.[31] For generation of baculoviral constructs first the coding sequence of the *B*. *mori* fibroin light chain protein (FLC) including its signal sequence (NM_001044023.1) was synthesized by MWG (Eurofins MWG Operon, Ebersberg, Germany) and cloned into the pFastBac/NT-TOPO vector system (Invitrogen, Thermo Fisher Scientific Inc., Basel, Switzerland). The resulting vector was termed pFastBac-FLC. This vector DNA then was linearized with restriction enzymes BamHI and XhoI (Fermentas, Thermo Fisher Scientific Inc.) and further used for cloning of the FLC-GDF-6 and FLC -TGF-β3 fusion constructs.

Naturally, the growth factors GDF-6 and TGF-β3 are expressed as pre-proteins with a long pro-domain and a signal peptide. During the processing into mature biologically active forms two pro-forms build a dimer and this dimer than is stabilized by a disulfide bridge. Then, at the cell membrane the active dimer is cut from the pro-domain and released from the cell as a bioactive dimer of GDF-6 or TGF-β3. Therefore, for functionalization of the silk fibroin with an active GDF-6 or TGF-β3 dimer, which would not be processed and cut off, it was necessary to generate an artificial dimer. Thus, two DNA sequences of each of the monomer peptides (sources: GDF-6, NM_001001557.3 and TGF-β3, NM_003239.2) were synthesized by MWG (Eurofins MWG Operon) and fused together using a two-step cloning strategy. As a first step, one peptide called “mature 1” [BamHI site – Linker (20 aa) – mature GDF-6 (120 aa) or TGF-β3 (112 aa) sequence –XhoI site] was inserted into the BamHI/XhoI linearized pFastBac-FLC vector. In a second step, the vectors containing already mature peptide 1 were linearized again using XhoI and SpHI. The second peptide “mature 2” [XhoI site –

Linker (20 aa) – mature GDF-6 (120 aa) or TGF-β3 (112 aa) sequence –SpHI site] was then ligated into the vector and after transformation the final vectors pFastBacFLC-GDF-6 and pFastBacFLC-TGF-β3 could be used for virus production according the "Bac-to-Bac TOPO Expression System" protocol (Thermo Fisher Scientific Inc.).
For production of transgenic silkworm larvae, *B. mori* larvae were infected with FastBacFLC-GDF-3 or FastBacFLC-TGF-β3 viruses by injecting 100 µL of virus, having a titer of 108 pfu/mL under sterile conditions. After infection, larvae were returned to germfree conditions. After seven days, larvae were dissected and mature silk fibroin was extracted from silk glands as described in Rheinnecker et al. (2012)[32]. Liquid silk was then collected under the microscope and aseptic conditions. Silk membrane-fleece composites were spun according to pre-established protocols.[29] 1) silk with human recombinant growth and differentiation factor 6 (GDF-6-silk), 2) silk with transforming growth factor β3 (TGF-β3-silk) and 3) silk without growth factor (cSilk). Silk 2 and 3 acted as controls for the GDF-6-silk. GDF-6 was shown to transform hMSC towards a disc-phenotype[23,24,33] and TGF-β3-Silk is expected to induce a more chondrogenic differentiation.[34] Presence of target growth factors were demonstrated by Western blotting before proceeding to *in vitro* cytocompatibility assays (see Fig. S1).

Experimental set-up

Silk scaffolds were cut in 5x5 mm^2 pieces and distributed into 48-well plates with one silk scaffold per well. Then 120,000 cells, either hAFC or hMSC, were added to the fleece side of the scaffold. After 30 minutes of attachment High Glucose DMEM (HG-DMEM) supplemented with 1% non-essential amino acids, 1% ITS+, 50 µg/ml ascorbic acid and 100 nM dexamethasone was added to the wells. For the exogenous growth factor groups (exGDF-6 and exTGF-β1) medium with either 100 ng/ml GDF-6

(PeproTech Inc., London, UK) or 10 ng/ml TGF-β1 (PeproTech Inc.) was prepared. Media was replaced every two to three days.

Cytocompatibility

Cytocompatibility of the different silk scaffolds was tested by metabolic activity, live/dead assay and imaging by scanning electron microscope (SEM). For mitochondrial activity 120,000 hMSC (passage two) were seeded on a square-shaped 5x5 mm^2 silk scaffold and cultured up to 21 days in HG-DMEM supplemented with 10 % FCS (Fig. 1). On day one, seven, 14 and 21 the scaffolds were immersed in 50 µM resazurin sodium salt solution supplemented to the HG-DMEM containing 10 % FCS (Sigma-Aldrich) and incubated for two hours at 37 °C. Fluorescence was measured at an excitation wavelength of 544 nm and an emission wavelength of 578 nm using an ELISA reader (Spectramax M5, Molecular Devices, distributed by Bucher Biotec, Basel, Switzerland).

Live/dead assay was performed on day one, seven, 14 and 21 by staining living cells with 2 µM calcein-AM and 7.1 µM DAPI (Sigma-Aldrich) in serum-free HG-DMEM for 1.5 hours at 37 °C. Subsequently, images were taken on a confocal laser scanning microscope (cLSM, cLSM710, Carl Zeiss, Jena, Germany) to create 3D stacks of the scaffolds at 10x magnification. Moreover, hMSC were seeded onto 5x5 mm^2 scaffolds for seven days. After two washing steps with phosphate buffered saline (PBS) samples were fixed with 2.5 % glutaraldehyde. Followed by post fixation with 1 % OsO_4 in 0.1 M cacodylate buffer (pH 7.4), critical point drying (Leica EM CPD300, Leica Microsystems, Heerbrugg, Switzerland) and sputter coating was performed with approximately 15 nm of gold (BalTec SCD004, Leica Microsystems). Images were

taken with a digital field emission scanning electron microscope DSM 982 Gemini (Carl Zeiss) at an accelerating voltage of 5 kV at a working distance of 6 - 8 mm. Fiber diameters were measured by using imageJ (1.48v, National Institute of Health, USA).

Extracellular matrix content

Prior determination of extracellular matrix production, mainly glycosaminoglycan (GAG), samples were digested with 3.9 U/mL papain from *Papaya latex* in a buffer containing 5 mM L-cysteine hydrochloride, 55 mM sodium citrate dihydrate, 150 mM sodium chloride and 5 mM EDTA (ethylene-diamine-tetra-acetic acid disodium salt dehydrate, all from Sigma-Aldrich). After spinning down undigested silk fibers supernatant was used to assess GAG and proteoglycan content using 1,9-dimethyl-methylene blue (Sigma-Aldrich) of technical duplicates. Determination is based on precipitation of GAG and proteoglycans with the positively charged dye.

DNA content

Papain digested samples were used to determine quantitated double-stranded DNA content using Quant-iT™ PicoGreen® dsDNA reagent (Thermo Fischer Scientific Inc.). In short, samples were mixed 1:1 with the diluted PicoGreen® reagent. Upon incubation for 2.5 min, fluorescence was measured at an excitation wavelength of 487 nm and an emission wavelength of 525 nm. Technical duplicates were performed.

Gene expression

Expression of major IVD catabolic (*ADAMTS5*, *MMP3* and *MMP13*), anabolic (*ACAN*, *VCAN*, *COL1A2* and *COL2A1*) and additionally several NP marker genes (*SOX9*, *KRT8* and *KRT19*) were determined using real-time reverse transcriptase quantitative polymerase chain reaction (qPCR) to assess inside-out repair processes (Table 1). For

this, scaffolds were snap-frozen in liquid nitrogen and mechanically pulverized using a mortar and pestle. Then, powder was suspended in 1 mL TRIzol Reagent® followed by addition of 5 µL of polyacryl carrier (both Molecular Research Center Inc., Cincinnati, USA). Phase separation was induced by addition of 1-bromo-3chloropropane (Sigma-Aldrich) and the clear phase was used for RNA isolation by GenElute™ Kit (Sigma-Aldrich). Residual DNA was degraded by DNase (DNase 1 Kit, Sigma-Aldrich) and reverse transcription was performed using iScript™ cDNA synthesis Kit (Bio-Rad Inc., Cressier, Switzerland). cDNA was then mixed with iTaq™ universal SYBR® Green supermix (Bio-Rad) with addition of a forward and reverse primer (Microsynth, Balgach, Switzerland) for each gene (Table 1). qPCR was performed in duplicates on a CFX96 Touch Real-Time PCR Detection System (Bio-Rad). Two reference genes, i.e. 18S and GAPDH, were used and relative gene expression was calculated using the $2^{-\Delta\Delta Ct}$ method[35] using the CFX Manager™ software version 3.1 (Bio-Rad).

Statistical analysis

Statistical analysis was performed using two-way ANOVA followed by Bonferroni's multiple comparisons test for mitochondrial activity, DNA and GAG content (given as mean ± SEM), one-way ANOVA followed by Bonferroni's multiple comparisons test for gene expression and fiber diameter (given as mean ± SEM). Further one sample *t*-test with a hypothetical value of one was used for gene expression and a 10-fold up- or down-regulation was considered biological relevant using GraphPad Prism version 6.0h (GraphPad Software, La Jolla, California, USA).

RESULTS

Silk scaffold

Imaging

Silk scaffolds were first examined macroscopically and then microscopically to obtain an overview, see Fig. 2A-D. In order to visualize fibers better a Keyence microscope (VHX5000) equipped with a Z20 zoom objective was used, see Fig. 2B. Thereby, no difference could be observed among the three silks. SEM imaging indicates that for all three different silk types fibers were uniform and displayed regular grooves, see Fig. 2B. The membrane side of all samples showed a flat surface with some elevations. These are also present on the control silk and hence cannot be attributed to the incorporated GF, see Fig. 2C.

When analyzing fiber diameters for GDF-6-silk (63.60 ± 2.82 μm) and TGF-β3-silk (67.13 ± 3.18 μm) they did not differ significantly ($p > 0.9999$). However, both differed significantly from cSilk (49.11 ± 1.75 μm, $p < 0.0001$).

Cell cytocompatibility

Cell activity was assessed using three different assays; mitochondrial activity, DNA content and live/dead stain (i.e. calcein-AM/ethidium homo-dimer staining, see Fig. 3). All assays attribute a very high cell cytocompatibility as shown by a significant increase of cellular activity and DNA content for both cell types (hAFC and hMSC) on all tested silk scaffolds.

Mitochondrial activity

Mitochondrial activity was measured by resazurin sodium salt assay and presented a continuing increase over 21 days for hMSC that was significantly higher than compared to day one: i.e. GDF-6-silk was increased from 1,657.00 ± 275.75 to 4,369.12 ±

1,558.04 RFU/scaffold (p = 0.0095), TGF-β3-silk was increased from 1,344.70 ± 198.38 to 4,038.70 ± 1,609.48 RFU/scaffold, (p = 0.0101) and cSilk with exogenous GDF-6 from 1,153.18 ± 226.06 to 4,967.24 ± 1,714.59 RFU/scaffold (p = 0.0002) (Fig. 4A). The same significant increase could be observed for hAFC on day 21 vs. day one for cSilk (from 1,647.18 ± 304.26 to 5,559.11 ± 1,593.74 RFU/scaffold), for GDF-6-silk (from 1,643.6013 ± 263.76614 to 5,310.79 ± 1,228.44 RFU/scaffold), for TFG-β3-silk (from 3.07 ± 1.25 to 62,156.00 ± 2,291.86 RFU/scaffold), and finally for cSilk with exogenous TGF-β1 (from 2.80 ± 0.71 to 5,907.86 ± 927.46 RFU/scaffold) (for all these comparisons $p < 0.0001$) and for cSilk with exogenous GDF-6 (from 3.38 ± 0.71 to 3,427.07 ± 1,520.23 RFU/scaffold, p = 0.0214) (Fig. 4B). Cell metabolic activity among the different silk types did not differ significantly when seeded with hMSC (p = 0.3235) whereas for hAFC a small significant effect among silk scaffolds was observed (p = 0.0453) (Fig. 4A-B).

DNA content

To assess cell proliferation DNA content was determined over culture period and among silk types (Fig. 4C-D). In all samples with hMSC a significant DNA content increase was obtained compared to day 14 and 21, respectively (Fig. 4C). For cSilk (d1 vs. d14) a significant increase was observed from 5.97 ± 2.48 to 11.66 ± 4.39 ng/scaffold (p = 0.0041, Fig. 4C) and for day one vs. day 21 for GDF-6 (from 4.04 ± 0.50 to 15.95 ± 6.19 ng/scaffold) and TGF-β3-silk (from 3.07 ± 1.25 to 16.67 ± 8.14 ng/scaffold) as well as exogenous GFD-6 (from 3.38 ± 0.71 to 15.96 ± 7.65 ng/scaffold) $p < 0.0300$. From day 14 to day 21 a trend was revealed towards a decreasing DNA content except for the cSilk with exogenous TGF-β1 stimulation (from 2.79 ± 0.71 to 5.29 ± 2.60 ng/scaffold), see Fig. 4C. We assume that the high cell concentration on the

silk scaffolds hindered further cell proliferation hence the decrease of DNA content. Due to the increasing cell viability of fewer cells we concluded that the cells progress from proliferation towards differentiation. In hAFC samples a more stable DNA content was observed showing a trend towards increase over culture period. In the exogenous TGF-β1 group significant DNA increase could be observed for day one (1,594.56 ± 299.86 ng/scaffold) vs. day 14 (5,657.35 ± 1,893.40 ng/scaffold) and day 21 (5,907.86 ± 927.46 ng/scaffold) ($p < 0.0001$), see Fig. 4D.

Live/Dead staining

Live/dead staining revealed an autofluorescence of silk in the red and partial in the blue channel. Hence detection of dead cells with ethidium homodimer or via exclusion using DAPI was not meaningful. A high number of living cells were found mainly along the silk fibers where they proliferated, see Fig. 3. Based on the calcein-AM stain we could not find differences in cell numbers of the different silk scaffolds. All seeded cells were continuously proliferating on all three scaffolds.

Differentiation of hMSC

To investigate whether hMSC differentiated towards a NP-like phenotype two analysis were performed: 1) determination of the GAG/DNA ratio and 2) gene expression of IVD marker genes and more precisely the ratio of *ACAN* to *COL2*.

GAG/DNA ratio

The GAG/DNA ratio is a measure of extracellular matrix production per amount of DNA and is an indication of differentiation towards a disc phenotype. We could observe a significant increase over 21 days with hMSC on GDF-6-silk from 4.72 ± 3.02 to 25.68 ± 18.53, $p = 0.0370$. hMSC cultured on cSilk with exogenous GDF-6 stimulation increase from 7.21 ± 5.00 to 17.55 ± 11.30 ($p = 0.9837$) and cSilk from 5.22 ± 2.95 to

13.91 ± 9.37, TGF-β3-silk from 0.21 ± 0.21 to 7.17 ± 2.76 and cSilk with exogenous TGF-β1 stimulation from 19.61 ± 7.72 to 9.82 ± 8.74, (all $p > 0.9999$) see Fig. 4E.
In the groups with hAFC a more stable ratio was observed over the culture period with non-significant increase of GAG/DNA ratio for cSilk from 0.29 ± 0.03 to 0.26 ± 0.08, cSilk with exogenous GDF-6 stimulation from 0.27 ± 0.06 to 0.39 ± 0.33 and cSilk with exogenous TGF-β1 stimulation from 0.17 ± 0.09 to 0.10 ± 0.02 all $p > 0.9999$. hAFC on GDF-6-silk from 0.38 ± 0.08 to 0.07 ± 0.03, $p = 0.5311$ and TGF-β3-silk from 0.31 ± 0.09 to 0.06 ± 0.02 ($p = 0.8528$).

Gene expression

Gene expression revealed, that both the *ACAN*/*COL2* ratio as well as the *COL1*/*COL2* ratio of hMSC and hAFC did not show a significant difference among silk scaffold in one-way ANOVA. Nevertheless, a more than 10-fold up-regulation in *ACAN*/*COL2* for hMSC was observed for GDF-6 (12.00) and TGF-β3-silk (13.80) whereas for *COL1*/*COL2* the silks with exogenous addition of GDF-6 (30.21) and TGF-β1 (10.07) showed biological relevant up-regulation, Fig. 5.

Additionally, other genes relevant for IVD were investigated. When comparing metalloproteinases (*MMP3*, *MMP13* and *ADAMTS5*) only in hAFC *MMP13* showed significant differences among silk scaffolds (one-way ANOVA $p = 0.0010$, cSilk, GDF-6-silk, TGF-β3-silk, exGDF-6 vs. exTGF-β1 $p < 0.0040$). When looking at relevant up-regulation exogenous stimulation with TGF-β1 caused higher up-regulation of catabolic genes in hAFC (*MMP3* [47.16-fold] and *MMP13* [29.72-fold]) except for *ADAMTS5* where exogenous stimulation with TGF-β1 showed 18.24-fold down-regulation. Also for hMSC a bigger up-regulation for *MMP13* was observed in TGF-β3-silk (42.05-

fold), exogenous stimulation with GDF-6 (21.75-fold) and TGF-β1 (1,092-fold), see Fig. 6.

Further, anabolic genes as *COL1*, *COL2*, *ACAN*, *VCAN* and *SOX9* were analyzed. Only for SOX9 significant difference among scaffolds could be observed. For hAFC one-way ANOVA resulted in $p = 0.0122$ with differences amongst cSilk vs. exTGF-β1 $p = 0.0462$, GDF-6 and TGF-β3-silk vs. exTGF-β1 $p < 0.0200$). Also for hMSC, *SOX9* showed differences amongst silks with one-way ANOVA $p = 0.0355$ for GDF-6, TGF-β3- and exGDF-6 vs. exTGF-β1 $p < 0.0470$. In the case of hMSC all silk scaffolds showed a down-regulation bigger than 10-fold except exTGF-β1. For *VCAN* we see a high up-regulation on all scaffold (> 300-fold) whereas hAFC showed no relevant changes. For *ACAN* and *COL1* no significant changes were observed. Nevertheless, Differences can be seen for COL2 for both, hMSC and hAFC, higher up-regulation is observed for cSilk (15.53 and 15.63-fold) and exTGF-β1 (91.96 and 1,936.00-fold). Further, TGF-β3-silk with hMSC had a 10.49-fold up-regulation.

The cytokeratins 8 and 19 showed down-regulation for both hMSC and hAFC. For hMSC these were higher than 10-fold for KRT19 except for cSilk and also significant amongst scaffolds (one-way ANOVA $p = 0.0411$) with cSilk vs. exTGF-β1 $p = 0.0339$. Also for hAFC the TGF-β1 group stood out with a 13.70-fold down-regulation. For KRT8 shows significant difference between cSilk and exTGF-β1 ($p = 0.0473$) but otherwise no relevant up- or down-regulation.

DISCUSSION

Silk scaffold

Although it seemed that on the GDF-6-silk slightly more cells were present when examining by SEM this probably arose from a small difference in initial seeding cell number. The difference in fiber diameter from cSilk to GDF-6-silk and TGF-β3-silk seemed not to affect cell adhesion or proliferation. Nevertheless, the density of the fleece differed among samples possibly resulting in somewhat different amounts of GF available for cells. To take this into account samples were chosen to show a fleece of similar density. Although, we did not observe differences among the scaffolds, for a pre-conditioning of cells to be transplanted or direct implantation for IVD repair this would have to be standardized to ensure consistent results. However, the production of silk fleece followed previously established protocols.[29,32,36] Besides the mentioned issue with fleece density the use of this scaffolds has several advantages about natural silk scaffolds. The main advantage is the covalently bound GF. By that measure, a slow release over an extended period of time can be achieved. Whereas a burst release and a higher GF concentration can be avoided. This is of high importance as negative side effects of overdosed GFs mainly BMP-2 from spinal fusion is under suspicion to correlate with a higher cancer incidence rate.[37,38] Moreover, fabrication of the scaffolds used in this study does not require steps to remove sericin from the silk fibroin as often done for different silk scaffold.[13,16-18] Instead the silk is directly isolated from the silk glands and renders further treatments to remove sericin unnecessary.

Cell cytocompatibility

Mitochondrial activity of hMSC as well as hAFC increased significantly from day one to day 21 on GDF-6-silk (hMSC $p = 0.0095$; and hAFC $p < 0.0001$, respectively), TGF-β3-silk (hMSC $p = 0.0101$; and hAFC $p < 0.0001$, respectively), cSilk with exogenous GDF-6 (hMSC $p = 0.0002$; and hAFC $p = 0.0214$, respectively) and exogenous TGF-β1 for hAFC ($p < 0.0001$). For cSilk a non-significant decrease from day 21 to day 14 could be observed. This might have been caused by cells reaching confluency and hence reduced mitochondrial activity. These outcomes already suggest that biocompatibility on all tested silk scaffolds is high. Also, as before for cSilk we observed a trend towards a decrease in DNA content from day 14 to day 21 on all silk scaffolds except cSilk with exogenous TGF-β1. This indicates, as the previously reduced mitochondrial activity, that cells nearly reached confluency. By performing live/dead assay we could visualize that cells were proliferating along silk fibers. Further, we observed that on day 14 and 21 the cells covered nearly all fiber surface what is again in accordance with mitochondrial activity and DNA content measurements. Hence, we attribute a high biocompatibility to the silk scaffolds tested.[39] This is consistent with results from other groups e.g. Panilaitis et al. (2003).[40] Also, silk scaffolds produced from the same supplier showed previously very good cytocompatiblity.[41]

Differentiation of hMSC and maintenance of hAFC

When comparing GAG/DNA ratio of hMSC and hAFC a trend towards an increased ratio, see Fig. 4, in hMSC was observed. HAFC, however, did not show any changes. This arose from the fact, that hAFC from the beginning on showed an approximately five times higher GAG content than hMSC causing overall a lower GAG/DNA ratio.

Our findings concerning the down-regulation of *KRT19* and *KRT8* as well as the significant decrease in *ACAN*/*COL2* ratio in the group with exogenous addition of TGF-β1 is in congruence with previously reported studies comparing the outcome of application of either TGF-β1 or GDF-5.[34,42] The *ACAN*/*COL2* ratio, which was proposed as one of the NP phenotype markers[43,44] showed a favorable ratio for NP-like cells for hMSC on the GF-enriched silk with GDF-6 (12-fold increased) and TGF-β3 (13.80-fold increase) but not for the exogenous stimulation with TGF-β1, where the ratio was inverted as previously observed.[34,42] A further limit of this study was the lacking experimental group of exogenous stimulation with TGF-β3. It has been demonstrated that TGF-β3 seems to be the more favorable cytokine for IVD repair.[45,46] However, historically TGF-β1 has been used much more widely to induce chondrogenic differentiation.[47,48] In our data the different action of TGF-β1 is evident, as GAG production seems merely blocked compared to stimulation with GDF-6[23] or similarly to GDF-5. Also, when comparing to the *COL1*/*COL2* ratio the silk with exogenous stimulation shows an increase in *COL1* production. Suggesting differentiation to a less desired phenotype. When looking at hAFC that act as a control we could not observe either a positive or negative change in gene expression of these two ratios. When focusing on catabolic genes mainly the TGF-β3-silk and the exTGF-β1 scaffold showed biological relevant up-regulation of these marker genes for hMSC and hAFC. cSilk, GDF-6-silk and exogenous stimulation with GDF-6 seemed not to affect catabolic processes and seem to possess a higher cytocompatibility. This is also in accordance with mitochondrial activity, DNA content and LIVE/DEAD assay. Anabolic genes showed biological up-regulation for GDF-6-silk for hMSC (*ACAN*, *VCAN*) and showed down-regulation for *SOX9* and *KRT19*. Whereas, hAFC did not show changes for these

genes on GDF-6-silk scaffolds. Although the differentiation potential of this novel silk scaffold containing GDF-6 is not as high as expected administration of the GF occurs over a prolonged time and is locally fixed. Hence, systemic effects can be minimized which might arise by an initial burst release. This could be confirmed by determining GF release, Fig. S2. Further, the native hAFC did not seem to be negatively affected when seeded on the silk scaffolds. This makes this novel GDF-6-silk scaffolds a possible substrate to expand and differentiate cells e.g. autologous MSCs that then can be used later in an IVD repair treatment.

ACKNOWLEDGMENTS

This project was supported by the Gebert Rüf Foundation # GRS-028/13 and by partial funds from the Swiss National Science Foundation project # 310030_153411. We thank Eva Roth for her valuable assistance in cell isolation and biochemical assays. Imaging was performed on equipment of the Microscopy Imaging Center (MIC) facility, University of Bern and the kind support of the VetSuisse Faculty, University of Bern. W.M. was affiliated with Spintec Engineering GmbH, Aachen, Germany. We have no other conflicts of interest to disclose.

REFERENCES

1. Benneker LM, Andersson G, Iatridis JC, et al. 2014. Cell therapy for intervertebral disc repair: advancing cell therapy from bench to clinics. Eur Cell Mater 27:5-11.

2. Boubriak OA, Watson N, Sivan SS, et al. 2013. Factors regulating viable cell density in the intervertebral disc: blood supply in relation to disc height. J Anat 222:341-348.

3. Shirazi-Adl A, Taheri M, Urban JP. 2010. Analysis of cell viability in intervertebral disc: Effect of endplate permeability on cell population. J Biomech 43:1330-1336.

4. Li Z, Peroglio M, Alini M, et al. 2015. Potential and limitations of intervertebral disc endogenous repair. Curr Stem Cell Res Ther 10:329-338.

5. Sakai D, Nishimura K, Tanaka M, et al. 2015. Migration of bone marrow-derived cells for endogenous repair in a new tail-looping disc degeneration model in the mouse: a pilot study. Spine J 15:1356-1365.

6. MacIntosh AC, Kearns VR, Crawford A, et al. 2008. Skeletal tissue engineering using silk biomaterials. J Tissue Eng Regen Med 2:71-80.

7. Shen X, Zhang Y, Gu Y, et al. 2016. Sequential and sustained release of SDF-1 and BMP-2 from silk fibroin-nanohydroxyapatite scaffold for the enhancement of bone regeneration. Biomaterials 106:205-216.

8. Berlemann U, Schwarzenbach O. 2009. An injectable nucleus replacement as an adjunct to microdiscectomy: 2 year follow-up in a pilot clinical study. Eur Spine J 18:1706-1712.

9. Kim JH, Kim DK, Lee OJ, et al. 2016. Osteoinductive silk fibroin/titanium dioxide/hydroxyapatite hybrid scaffold for bone tissue engineering. Int J Biol Macromol 82:160-167.

10. Park HJ, Lee OJ, Lee MC, et al. 2015. Fabrication of 3D porous silk scaffolds by particulate (salt/sucrose) leaching for bone tissue reconstruction. Int J Biol Macromol 78:215-223.

11. Meinel L, Karageorgiou V, Hofmann S, et al. 2004. Engineering bone-like tissue in vitro using human bone marrow stem cells and silk scaffolds. J Biomed Mater Res A 71:25-34.

12. Melke J, Midha S, Ghosh S, et al. 2016. Silk fibroin as biomaterial for bone tissue engineering. Acta Biomater 31:1-16.

13. Du L, Zhu M, Yang Q, et al. 2014. A novel integrated biphasic silk fibroin scaffold for intervertebral disc tissue engineering. Materials Letters 117:237 - 240.

14. Neo PY, Shi P, Goh JC, et al. 2014. Characterization and mechanical performance study of silk/PVA cryogels: towards nucleus pulposus tissue engineering. Biomed Mater 9:065002.

15. Hu J, Chen B, Guo F, et al. 2012. Injectable silk fibroin/polyurethane composite hydrogel for nucleus pulposus replacement. J Mater Sci Mater Med 23:711-722.

16. Bhattacharjee M, Miot S, Gorecka A, et al. 2012. Oriented lamellar silk fibrous scaffolds to drive cartilage matrix orientation: towards Annulus Fibrosus tissue engineering. Acta Biomater 8:3313-3325.

17. Park SH, Gil ES, Cho H, et al. 2012. Intervertebral disk tissue engineering using biphasic silk composite scaffolds. Tissue Eng Part A 18:447-458.

18. See EY, Toh SL, Goh JC. 2012. Simulated intervertebral disc-like assembly using bone marrow-derived mesenchymal stem cell sheets and silk scaffolds for annulus fibrosus regeneration. J Tissue Eng Regen Med 6:528-535.

19. Chang G, Kim HJ, Kaplan D, et al. 2007. Porous silk scaffolds can be used for tissue engineering annulus fibrosus. Eur Spine J 16:1848-1857.

20. Merrit JL. 1993. Silk: history, cultivation, and processing. Silk: Harper's Ferry Regional Textile Group, 11th Symposium, November 12-13, 1992, National Museum of American History. Harper's Ferry Regional Textile Group. United States.

21. Hofmann S, Foo CT, Rossetti F, et al. 2006. Silk fibroin as an organic polymer for controlled drug delivery. J Control Release 111:219-227.

22. Colombier P, Clouet J, Boyer C, et al. 2016. TGF-β1 and GDF5 act synergistically to drive the differentiation of human adipose stromal cells toward nucleus pulposus-like cells. Stem Cells 34:653-667.

23. Clarke LE, McConnell JC, Sherratt MJ, et al. 2014. Growth differentiation factor 6 and transforming growth factor-beta differentially mediate mesenchymal stem cell differentiation, composition and micromechanical properties of nucleus pulposus constructs. Arthritis Res Ther 16:R67.

24. Williams LA, Wei A, Bhargav D, et al. 2014. Cartilage derived morphogenetic protein 2 - A potential therapy for intervertebral disc regeneration? Biologicals 42:65-73.

25. Malonzo C, Chan SC, Kabiri A, et al. 2015. A papain-induced disc degeneration model for the assessment of thermo-reversible hydrogel-cells therapeutic approach. J Tissue Eng Regen Med 9:E167-E176.

26. Feng C, Liu H, Yang Y, et al. 2015. Growth and differentiation factor-5 contributes to the structural and functional maintenance of the intervertebral disc. Cell Physiol Biochem 35:1-16.

27. Liu W, Zhang Y, Feng X, et al. 2016. Inhibition of microRNA-34a prevents IL-1β-induced extracellular matrix degradation in nucleus pulposus by increasing GDF5 expression. Exp Biol Med (Maywood) 241:1924-1932.

28. Solchaga LA, Penick K, Porter JD, et al. 2005. FGF-2 enhances the mitotic and chondrogenic potentials of human adult bone marrow-derived mesenchymal stem cells. J Cell Physiol 203:398-409.

29. Wöltje M, Böbel M, Rheinnecker M, et al. 2014. Transgenic protein production in silkworm silk glands requires cathepsin and chitinase of Autographa californica multicapsid nucleopolyhedrovirus. Appl Microbiol Biotechnol 98:4571-4580.

30. Kato T, Kajikawa M, Maenaka K, et al. 2010. Silkworm expression system as a platform technology in life science. Appl Microbiol Biotechnol 85:459-470.

31. Teh TK, Toh SL, Goh JC. 2010. Optimization of the silk scaffold sericin removal process for retention of silk fibroin protein structure and mechanical properties. Biomed Mater 5:35008.

32. Rheinnecker M, Kohlhaas S, Zimmat R. 2012. Method and apparatus for extraction of arthropod gland. *United States Patent* US 8 105:B2.

33. May RD, Tekari A, Frauchiger DA, et al. 2017. Efficient non-viral transfection of primary intervertebral disc cells by electroporation for tissue engineering application. Tissue Eng Part C Methods 23:30-37.

34. Gantenbein-Ritter B, Benneker LM, Alini M, et al. 2011. Differential response of human bone marrow stromal cells to either TGF-β(1) or rhGDF-5. Eur Spine J 20:962-971.

35. Livak KJ, Schmittgen TD. 2001. Analysis of relative gene expression data using real-time quantitative PCR and the 2(-Delta Delta C(T)) Method. Methods 25:402-408.

36. Wöltje M, Böbel M. 2017. 12 - Natural biodegradable medical polymers: Silk, In Science and Principles of Biodegradable and Bioresorbable Medical Polymers, Zhang X. (eds). Woodhead Publishing; 351 - 376 p.

37. James AW, LaChaud G, Shen J, et al. 2016. A Review of the clinical side effects of Bone Morphogenetic Protein-2. Tissue Eng Part B Rev 22:284-297.

38. Bains R, Mitsunaga L, Kardile M, et al. 2017. Bone morphogenetic protein (BMP-2) usage and cancer correlation: an analysis of 10,416 spine fusion patients from a multi-center spine registry. J Clin Neurosci 43:214-219.

39. Frauchiger D, Heeb S, Tekari A, et al. 2017. Intervertebral disc repair by a combination of genipin-enhanced fibrin hydrogel and growth factor-enriched silk-fleece. Proceedings of the ORS. 19-22 March, San Diego.

40. Panilaitis B, Altman GH, Chen J, et al. 2003. Macrophage responses to silk. Biomaterials 24:3079-3085.

41. Hanken H, Göhler F, Smeets R, et al. 2016. Attachment, viability and adipodifferentiation of pre-adipose cells on silk scaffolds with and without co-expressed FGF-2 and VEGF. In Vivo 30:567-572.

42. Stoyanov JV, Gantenbein-Ritter B, Bertolo A, et al. 2011. Role of hypoxia and growth and differentiation factor-5 on differentiation of human mesenchymal stem cells towards intervertebral nucleus pulposus-like cells. Eur Cell Mater 21:533-547.

43. Mwale F, Roughley P, Antoniou J. 2004. Distinction between the extracellular matrix of the nucleus pulposus and hyaline cartilage: a requisite for tissue engineering of intervertebral disc. Eur Cell Mater 8:58-63; discussion 63-4.

44. Risbud MV, Schoepflin ZR, Mwale F, et al. 2015. Defining the phenotype of young healthy nucleus pulposus cells: recommendations of the Spine Research Interest Group at the 2014 annual ORS meeting. J Orthop Res 33:283-293.

45. Risbud MV, Di Martino A, Guttapalli A, et al. 2006. Toward an optimum system for intervertebral disc organ culture: TGF-beta3 enhances nucleus pulposus and anulus fibrosus survival and function through modulation of TGF-beta-R expression and ERK signaling. Spine (Phila Pa 1976) 31:884-890.

46. Martin JT, Gullbrand SE, Mohanraj B, et al. 2017. Optimization of preculture conditions to maximize the *in vivo* performance of cell-seeded engineered intervertebral discs. Tissue Eng Part A [Epub ahead of print].

47. Shintani N, Hunziker EB. 2011. Differential effects of dexamethasone on the chondrogenesis of mesenchymal stromal cells: influence of microenvironment, tissue origin and growth factor. Eur Cell Mater 22:302-19; discussion 319-20.

48. Tekari A, Luginbuehl R, Hofstetter W, et al. 2015. Transforming growth factor Beta signaling is essential for the autonomous formation of cartilage-like tissue by expanded chondrocytes. PLoS One 10:e0120857.

Figure legends

Fig. 1. (A) Manufacture of engineered silk via transfer vector containing gene of interested, infection of *B*. *mori* after 4th moth and monitoring of successful transduction by GFP expression in the glands of *B*. *mori*. (B) Experimental set-up for cell cyto-compatibility and differentiation potential investigation. 120,000 hMSC or hAF cells, respectively, were seeded on either an engineered silk scaffold or on control silk (cSilk). Silk examined contained either no growth factor (cSilk), GDF-6 or TGF-β3. Additionally, cSilk with exogenous addition of GDF-6 and TGF-β1 was investigated. A was reprinted from Kato *et al*. (2010)[30] with permission from the publishers.

Fig. 2. (A) Macroscopic picture of 5x5 mm^2 silk fleece membrane composite. (B) Top-view picture of TGF-β3-silk scaffold (C) Scanning electron microscope (SEM) image of membrane side of TGF-β3 representative for all three silk types (D) SEM images of fleece side of control silk, GDF-6-silk and TGF-β3-silk (top-down) were taken at either 100x magnification (left) or 2000x (control silk and GDF-6-silk) and 5000x magnification (TGF-β3-silk).

Fig. 3. Live/Dead assay performed with 120,000 hMSC on 5x5 mm^2 engineered silk fleece-membrane composite. Green = calcein-AM, red = autofluorescence of silk; scale bar = 100 μm.

Fig. 4. Biochemical assays performed on hMSC (n = 5, left column) and hAF (n = 5, right column) cells on different silk scaffolds. (A-B) Metabolic Activity, (C-D), DNA content and (E-F) GAG content normalized to DNA content. To evaluate statistical significance a two-way RM ANOVA followed by Bonferroni's multiple comparisons test was performed, p-values: *** < 0.0006, ** < 0.0095, * < 0.046.

Fig. 5. Gene expression of *Aggrecan* to *Collagen 2* and *Collagen 1* to *Collagen 2* of hMSC (top) and hAF cells (bottom) genes for hMSC and hAF. One sample t-test with a hypothetical value of 1.0 was used, p-values: *** ≤ 0.0005, * < 0.048.

Fig. 6. Relative gene expression analysis of major anabolic and catabolic IVD genes and for cytokeratins for hMSC (left) and hAF (right). One sample t-test with a hypothetical value of 1.0 was used, p-values: *** ≤ 0.0005, ** < 0.01, * < 0.048.

Supplementary Figures

Fig. S1. Western Blots of Fibroin light chain growth factor fusion proteins. (A) transgenic expression of the 56 kDa Fibroin light chain hTGF-β3 fusion protein (arrow). Lane 1 protein marker, lane 2-3: TGF-β3-silk each 375 µg, lane 4: positive control (50 ng TGF-β3 mixed into 375 µg native silk, arrow head), lane 5: negative control (native silk). (B) Western Blot of 58 kDa Fibroin light chain-GDF-6 fusion protein (arrow). Lane 1 negative control (native silk), lane 2 and 9: protein marker, lane 3 positive control (20 ng recombinant GDF-6 mixed with 375 µg native silk, arrow head), lane 4–8: different batches of GDF-6-silk each 375 µg.

Fig. S2. Release of Growth factor measured over 28 days by immersion of three 5x5 mm^2 GDF-6-silk and TGF-β3-silk in PBS and incubation at 37 °C. On preset time points PBS was removed and stored at -80 °C until analysis and PBS was replenished. Analysis was performed with a commercial ELISA kit for human GDF-6 and TGF-β3 detection (Abbexa Ltd., Cambridge, UK). GDF-6 released into PBS was below detection limit of kit < 0.156 ng/ml where small amounts of TGF-β3 could be detected.

Table 1: List of primers used for the two-step qPCR. The annealing temperature was 61 °C.

Gene	Description	Forward primer (5'-3')	Reverse primer (3'-5')
18S	18S ribosomal RNA	CGA TGC GGC GGC GTT ATT C	TCT GTC AAT CCT GTC CGT GTC C
GAPDH	Glyceraldehyde-3-phosphate dehydrogenase	ATC TTC CAG GAG CGA GAT	GGA GGC ATT GCT GAT GAT
ACAN	Aggrecan	CAT CAC TGC AGC TGT CAC	AGC AGC ACT ACC TCC TTC
VCAN	Versican	GTC TCC TCC TCG GCT CTG	ACC TAA TGT TCT CGG CTG TTG
COL1A2	Collagen type I alpha 2 chain	GTG GCA GTG ATG GAA GTG	CAC CAG TAA GGC CGT TTG
COL2A1	Collagen type II alpha 1 chain	AGC AGC AAG AGC AAG GAG AA	GTA GGA AGG TCA TCT GGA
ADAMTS5	ADAM metallopeptidase with thrombospondin type 1 motif 5	GCT GTG CTG TGA TTG AAG A	TGC TGG TAA GGA TGG AAG A
MMP3	Matrix metallopeptidase 3	CAA GGC ATA GAG ACA ACA TAG A	GCA CAG CAA CAG TAG GAT
MMP13	Matrix metallopeptidase 13	AGT GGT GGT GAT GAA GAT	CTA AGG TGT TAT CGT CAA GTT
SOX9	SRY-box 9	GAG ACT TCT GAA CGA GAG	GGC TGG TAC TTG TAA TCC
KRT8	Keratin 8	CCA GGA GAA GGA GCA GAT	CGC CTA AGG TTG TTG ATG TA
KRT19	Keratin 19	TGT GTC CTC GTC CTC CTC	GCG GAT CTT CAC CTC TAGC

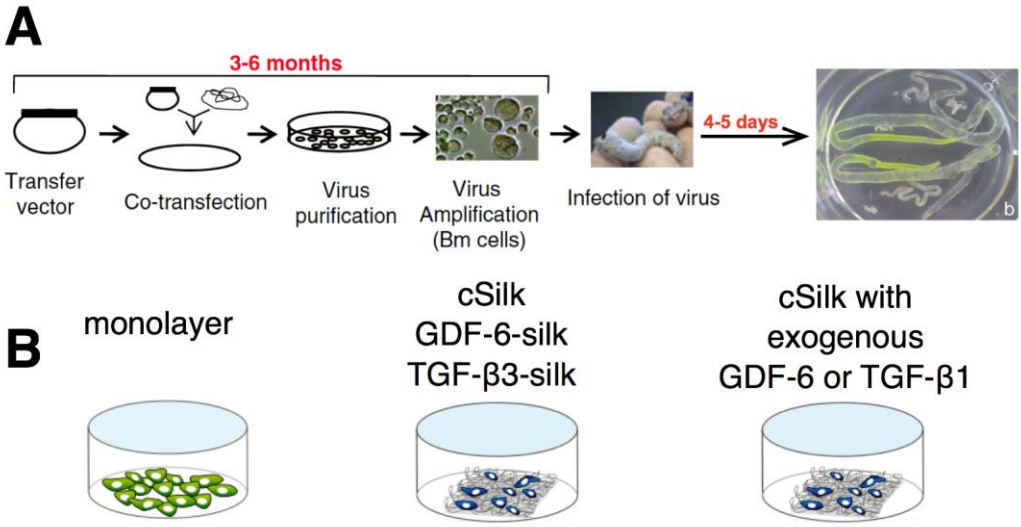

Figure 1

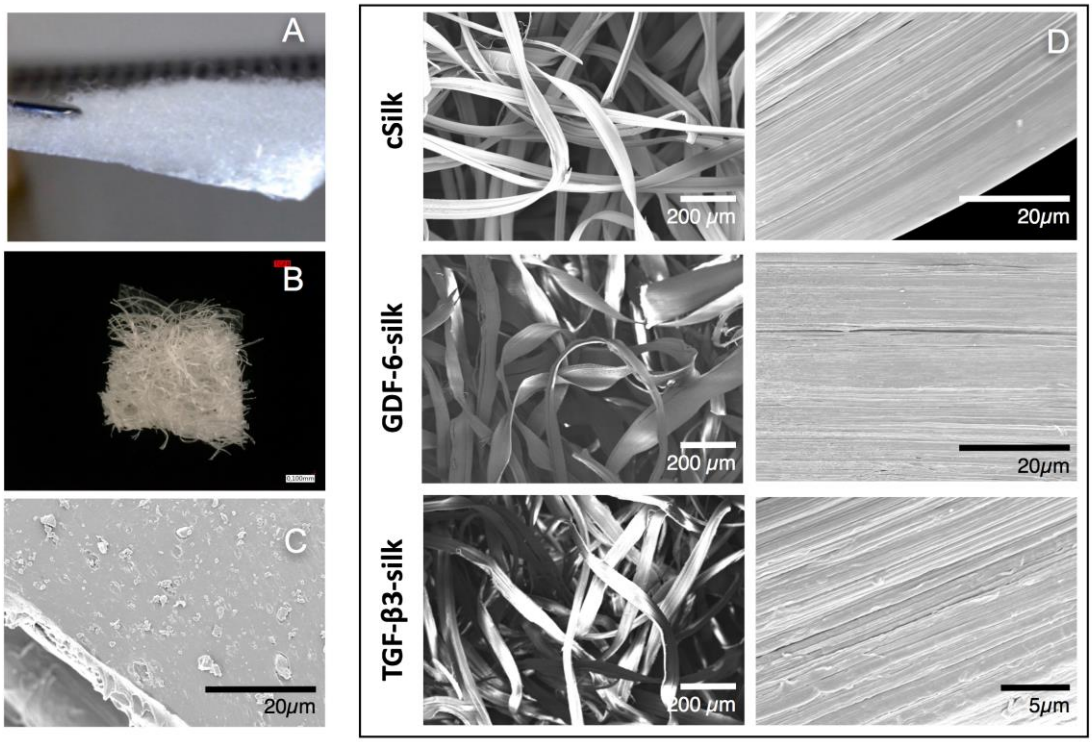

Figure 2

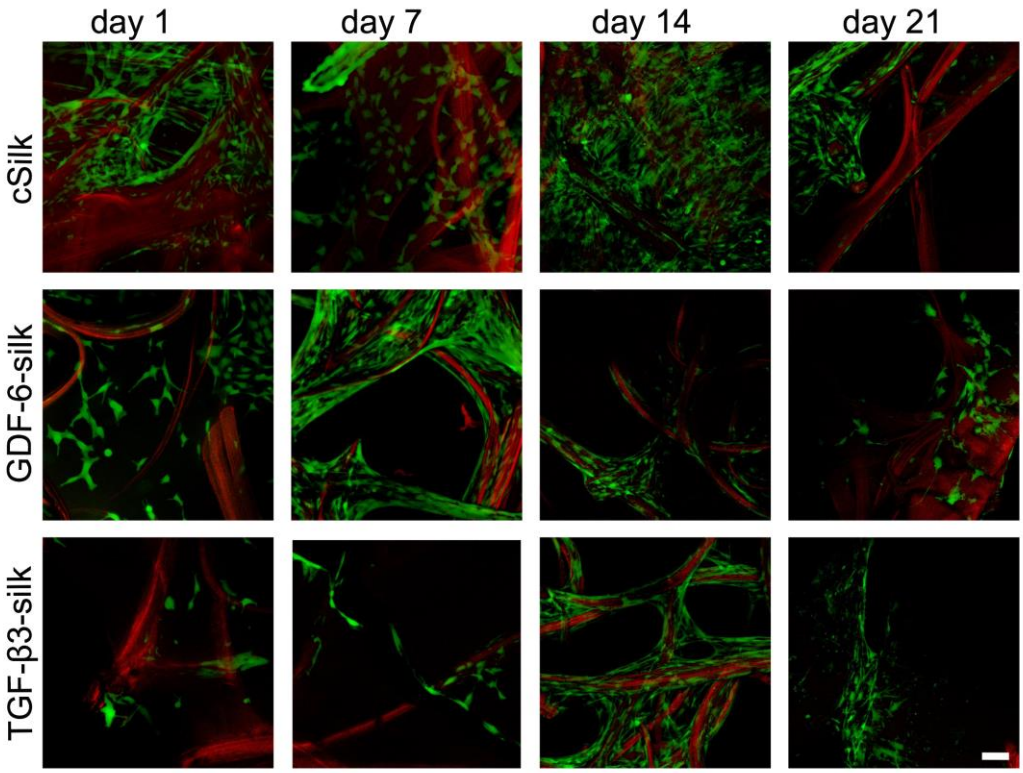

Figure 3

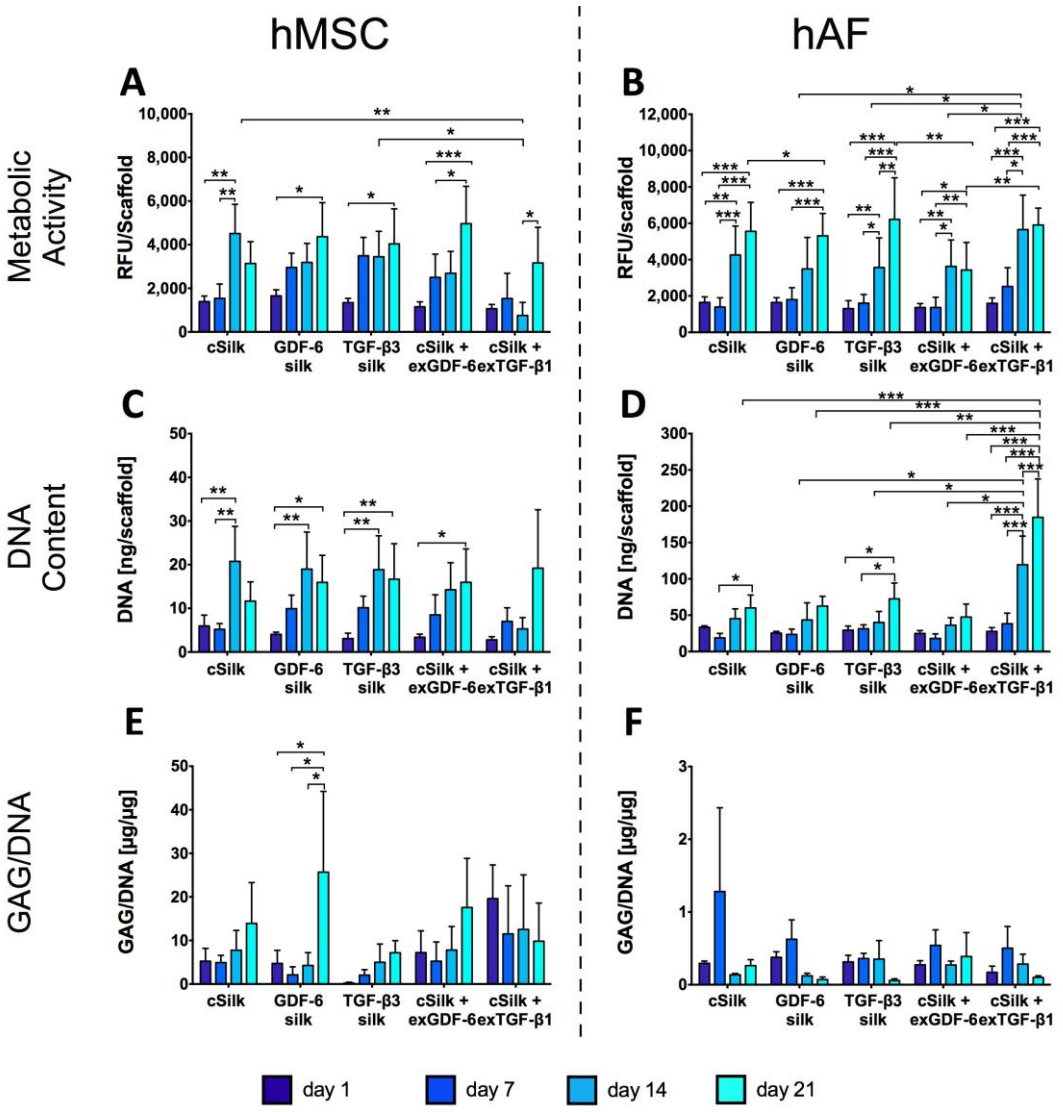

Figure 4

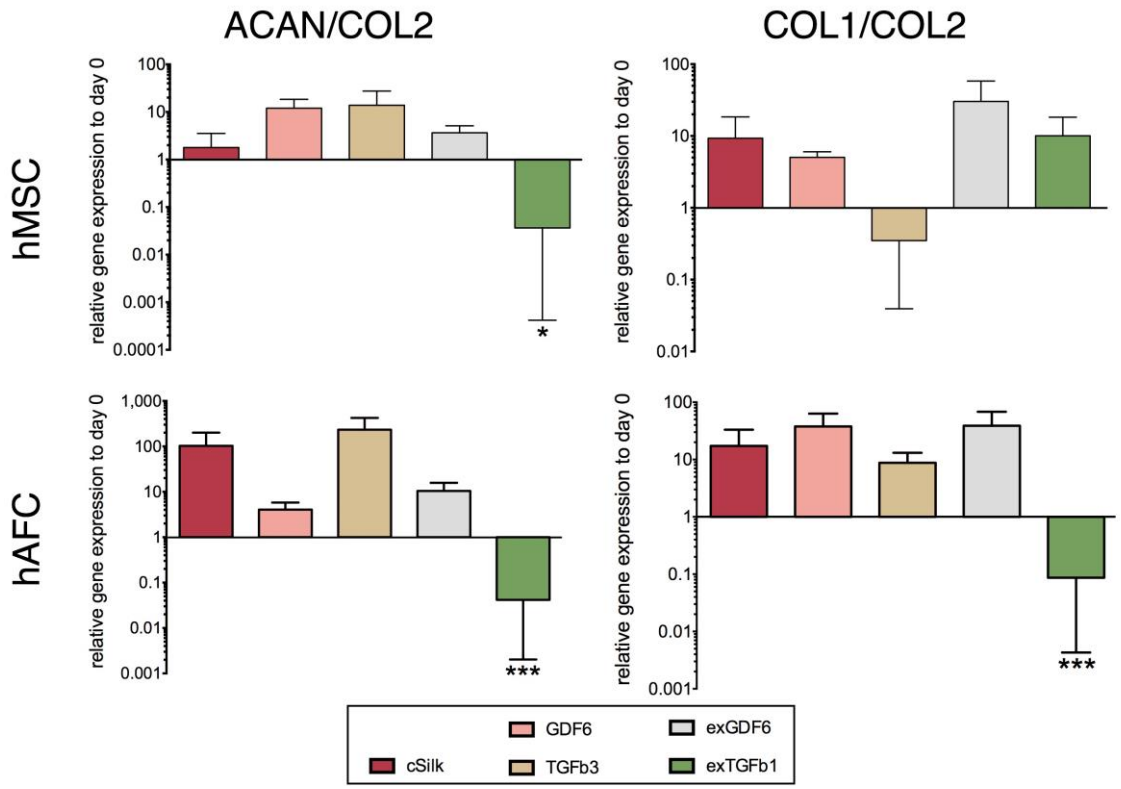

Figure 5

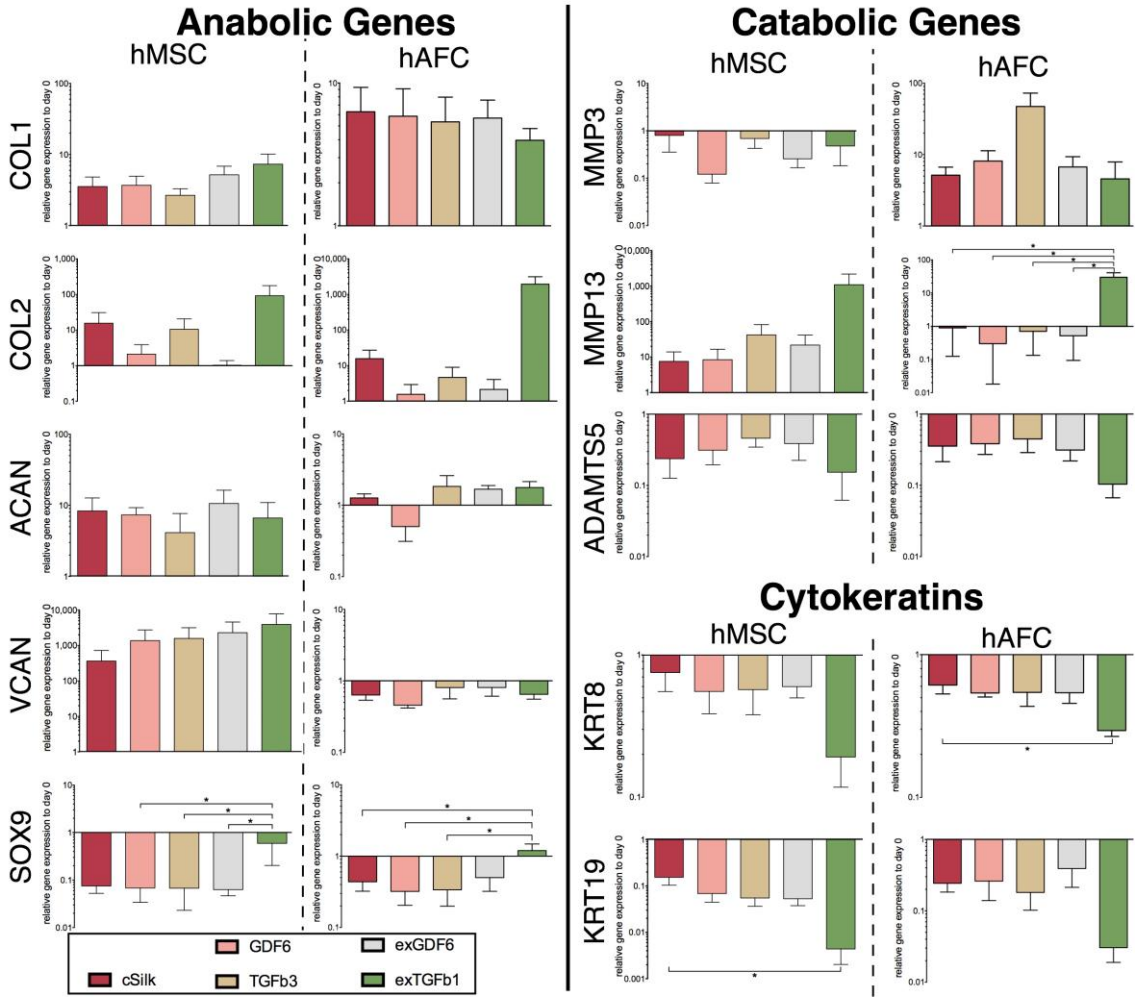

Figure 6